Front page

Title:

A leaf–level biochemical model simulating the introduction of C_2 and C_4 photosynthesis in C_3 rice: gains, losses and metabolite fluxes

Authors and addresses:

Chandra Bellasio[1–3*] and Graham D Farquhar[1]

[1]Research School of Biology, Australian National University, Acton, ACT, 2601 Australia;
[2]University of the Balearic Islands 07122 Palma, Illes Balears, Spain;
[3]Trees and Timber institute, National Research Council of Italy, 50019 Sesto Fiorentino (Florence).

ORCID:

0000-0002-3865-7521 (CB); 0000-0002-7065-1971 (GDF)

Correspondence details:

chandra.bellasio@anu.edu.au; +61(0)261255071

Word counts:

Summary: 200; Introduction to Conclusion: 6595.

Number of tables:

1

Figures:

6 (5 in colour).

Supporting information:

File 1: 25 pages, 10 notes, 9 figures, and 3 tables.

File 2: Methods S1: The model, coded in Excel, made freely available.

New Phytologist, Full paper

A leaf–level biochemical model simulating the introduction of C_2 and C_4 photosynthesis in C_3 rice: gains, losses and metabolite fluxes

Chandra Bellasio[1–3*] and Graham D Farquhar[1]

[1]Research School of Biology, Australian National University, Acton, ACT, 2601 Australia;
[2]University of the Balearic Islands 07122 Palma, Illes Balears, Spain;
[3]Trees and Timber institute, National Research Council of Italy, 50019 Sesto Fiorentino (Florence).

*Correspondence: chandra.bellasio@anu.edu.au

Summary:

- This work aims at developing an adequate theoretical basis for comparing assimilation of the ancestral C_3 pathway with CO_2 concentrating mechanisms (CCM) that have evolved to reduce photorespiratory yield losses.
- We present a novel model for C_3, C_2, C_2+C_4 and C_4 photosynthesis simulating assimilatory metabolism, energetics, and metabolite traffic at the leaf– level. It integrates a mechanistic description of light reactions to simulate ATP and NADPH production, and a variable engagement of cyclic electron flow. The analytical solutions are compact and thus suitable for larger scale simulations. Inputs were derived with a comprehensive gas exchange experiment.
- We show trade–offs in the operation of C_4 that are in line with ecophysiological data. C_4 has the potential to increase assimilation over C_3 at high temperatures and light intensities, but this benefit is reversed under low temperatures and light.
- We apply the model to simulating the introduction of progressively complex levels of CCM into C_3 rice, which feeds more than 3.5 billion people. Increasing assimilation will require considerable modifications such as expressing the NDH complex and upregulating cyclic electron flow, enlarging the bundle sheath, and expressing suitable transporters to allow adequate metabolite traffic. The simpler C_2 rice may be a desirable alternative.

Keywords

Stomata, enzyme, light limitation, C_2 shuttle, C_3–C_4 intermediate, photorespiration, bio–engineering, assimilation.

Running title

Simulating biochemical carbon concentrating mechanisms

Introduction

Carbon concentrating mechanisms (CCM; acronyms are listed in Table 1) are co–ordinated suites of structural and biochemical modifications to ancestral C_3 photosynthesis. CCMs evolved to reduce the magnitude of photorespiration, a complex process resulting in the release of previously fixed CO_2, which incurs substantial energy costs to recycle by–products (Meyer & Griffiths, 2013). In plants, CCMs have the form of biochemical cycles that increase the CO_2/O_2 ratio at the Rubisco catalytic site, and are of two types: the 'C_2 shuttle' and the C_4 cycle. To operate a CCM, the photosynthetic parenchyma is often differentiated into two cell types, although single–celled systems do exist (King *et al.*, 2012): an external layer of mesophyll (M) and an internal layer of bundle sheath (BS) encircling the vasculature (Lundgren *et al.*, 2014). The C_2 shuttle consists of the compartmentation of glycine decarboxylase (GDC) activity in the BS, delivering CO_2 around Rubisco in the BS, using the photorespiratory glycine produced in the M (Keerberg *et al.*, 2014). The C_4 cycle represents a further sophistication involving an energy dependent carboxylation–decarboxylation cycle. CO_2 is initially fixed into a four–carbon (C_4) organic acid (OAA) in the M by phosphoenolpyruvate carboxylase (PEPC), which after reduction (or transamination) diffuses to the BS where it is decarboxylated. If, on the one hand, the C_4 cycle lowers the photorespiratory ATP demand, on the other it requires a considerable amount of ATP (2 ATP per CO_2 pumped, for the NADP–ME subtype) for the regeneration of phosphoenolpyruvate (Kanai & Edwards, 1999; Evans *et al.*, 2007; Bellasio, 2017). In 'C_2+C_4' species (Bellasio, 2017) the degree of PEPC engagement, and the extent of Rubisco compartmentation to the BS are intermediate and are species dependent (Monson & Moore, 1989). In C_4 species, PEPC is fully engaged and CO_2 accumulates in the BS at concentrations that are 10– to 20–fold greater than ambient, thereby saturating a fully compartmentalised Rubisco in the BS (von Caemmerer & Furbank, 2003). The biochemical functions of the M and BS need to be separated by a suitable distance (Jurić *et al.*, 2017). Across this space large fluxes of metabolites need to be exchanged, both through plasmodesmata (Osmond & Smith, 1976; Danila *et al.*, 2018), and through a suite of chloroplast membrane transporters (Weber & von Caemmerer, 2010; Gowik *et al.*, 2011; Schlüter *et al.*, 2016).

Quantifying the potential gains from operating a CCM has challenged physiologists for the last 50 years. Simple approaches have compared C_3 and C_4 plants, but the evolutionary traits of unrelated species can differ substantially, preventing the isolation of the effects of CCMs [reviewed in Snaydon (1991) and Christin and Osborne (2014)]. For instance, in a large comparative experiment Atkinson *et al.* (2016) found C_3 and C_4 grasses mainly differed in terms of leaf mass per area, rather than net assimilation rate per unit leaf area, but Taylor *et al.* (2010) reported that a more limited set of C_4 grasses had a 45 % higher assimilation rate than C_3 grasses. The comparison is further complicated by the co–occurrence of acclimatory traits: Schmitt and Edwards (1981) reported that the effect of short and long term temperature acclimation was greater than any

difference in assimilation rate between maize and rice. Even in targeted comparisons between rice and the sympatric weed *Echinochloa glabrescens* or crops such as maize, results were inconclusive (Sheehy, 2007; Covshoff *et al.*, 2016). To quantify the benefit of operating a CCM it is therefore critical to compare two plants in which all traits, other than the strength of the CCM, are equal.

For this hypothetical analysis, mathematical models are in principle the ideal tool. Heckmann *et al.* (2013) found a smooth monotonic increase in assimilation for increasing levels of C_4 expression in a C_3 background. This finding was directly dependent on the assumption of unlimited ATP, and contrasts with the observation that C_4 plants are favoured only under high temperatures and light intensities (Monteith, 1978; Pearcy & Ehleringer, 1984). Wu *et al.* (2017) compared predictions of C_3 and C_4 models, but these were parameterised separately by curve fitting on representative C_3 and C_4 crops, thereby replicating the unwanted coexistence of multiple traits present in nature within the models. The light–limited model developed by von Caemmerer (2000) assumed a fixed stoichiometric conversion between electron transport and ATP production and is unsuitable for testing different levels of C_4 engagement because the C_4 cycle requires an increased ratio of ATP to NADPH, which C_4 plants obtain by upregulating cyclic electron flow, CEF (Ishikawa *et al.*, 2016). Recently Yin and Struik (2017) overcame some of these shortcomings, but biochemical processes were relatively schematic, and as a result, metabolite exchange requirements have not been quantified.

The aims of this work were three–fold. Firstly, to develop the theoretical underpinnings of the introduction of CCMs into C_3 crops at the leaf level; secondly, quantify the possible benefits and trade–offs of CCMs if they were to be made operational in rice; and, finally, estimate realistic fluxes to help define targets for expression of enzymes and transporters. Light–limited formulations working under the assumption of limiting ATP or NADPH, as well as enzyme–limited formulations, all valid for any photosynthetic type, are developed here. These are integrated with a mechanistic description of photosynthetic light reactions, and with a biochemical and hydromechanical model of stomatal behaviour. A gas–exchange experiment was used to inform the model. The results predict that introducing CCMs in C_3 metabolism under the current ambient CO_2 concentration would increase assimilation under full light, but the benefit would be reversed at low light intensity (*PPFD*). For C_4 photosynthesis, achieving this potential will require an appropriate electron transport chain, allowing adequate metabolite traffic, and enlarging the BS to house the biochemical and light harvesting machinery.

Material and Methods

Overview of the modelling approach

The modelling scheme is depicted in Figure 1 to highlight key inputs and outputs, This model was newly derived to allow a seamless transition between all photosynthetic types except CAM, and joins together an electron transport submodel, a biochemical submodel, a stoichiometric submodel (see schematic in Figure S1), and a stomatal submodel. The photosynthetic type is defined by setting the strength of the C_4 cycle [as PEP carboxylation rate ($V_{P(J)}$) in the light–limited model and maximum rate of PEPC, ($V_{P\,MAX}$) in the enzyme–limited submodel] together with the location of GDC (χ_{GDC}). The electron transport submodel (Note S1, Figure S2) calculates the flux of ATP and NADPH (J_{ATP} and J_{NADPH}) made available under a given *PPFD*. Here, the limitations of previous modelling approaches using a fixed stoichiometry of the electron transport chain (see *Introduction*) were resolved by allowing the ratio of ATP/NADPH production to be adjusted through mechanisms that were found to be critical in C_4 plants. These are the regulation of the rate of cyclic electron flow (CEF) through the parameter f_{Cyc}, and inducing the NAD(P)H Dehydrogenase–like (NDH) complex (Ivanov *et al.*, 2005; Friso *et al.*, 2010; Munekage *et al.*, 2010) which is characteristic of C_4, and not used by C_3 plants, operating mainly the PGR5 / PGRL1 pathway (Yamori & Shikanai, 2016) by varying f_{NDH} (the fraction of CEF passing through the NDH complex). The reducing power requirements of nitrogen reduction are implicitly accounted for here as pseudocyclic electron flow (lumped with the water–water cycle, and adjusted through $f_{Pseudocyc}$), in line with Yin and Struik (2012).

The biochemical submodel has different formulations depending on the limitation, sharing common underpinnings (Note S2). There is a formulation for limitation by Rubisco or PEPC carboxylating capacity (commonly referred to as enzyme limitation, Note S3) and two formulations for light–limited photosynthesis, derived under limiting ATP (Note S4) or NADPH (Note S5). Equations for triose phosphate limited photosynthesis (Busch *et al.*, 2018) were omitted for simplicity as they are relevant under low O_2 or high CO_2 concentrations, or low temperatures (Busch & Sage, 2017), while crops like rice – fertilised and irrigated – generally experience mainly light limitations (Yin & Struik, 2015). Similarly, limitations imposed by the diffusion of metabolites (Retta *et al.*, 2016) were neglected for simplicity, justified by a recent study addressing the introduction of a weak C_4 cycle in C_3 photosynthesis using a reaction diffusion model that found that any reduction of *A* due to the effect of diffusion processes was limited (Wang *et al.*, 2017). The ATP and NADH produced during respiration were neglected because they are likely to be consumed by basal metabolism, while NADH imbalances are likely to be dissipated by mitochondrial alternative oxidases (Buckley & Adams, 2011).

Using dummy values (initial values for a converging iteration) for the CO_2 concentration at the M carboxylating sites (C_M) the light–limited submodel calculates two distinct sets of outputs, under

NADPH and ATP limitations. Of those, that resulting in the minimum V_C is taken as output of the light–limited model. Similarly, starting from C_M, the enzyme–limited submodel calculates a full set of outputs using the kinetic characteristics of Rubisco and PEPC as inputs.

Outputs of light–limited and enzyme–limited submodels are joined using a smoothing function to give a continuous output (Note S6), as well as used to calculate τ, a quantity related to the ATP concentration in the M and the BS that acts as the biochemical driver of stomatal response (Note S7). This was included solely to realistically simulate stomatal conductance in a C_3 to C_4 continuum, but we make no claim about whether τ offers a faithful mechanistic description of stomatal behaviour. Hydro–mechanical forcing links guard cell responses to the water status and turgor of the leaf, which relate to soil water status and plant hydraulic conductance. The influence of biochemical factors relative to hydro–mechanical forcing is determined by the parameter β, while stomatal morphology is described by χ_S. The output of the stomatal submodel is stomatal conductance, (g_S) that, together with mesophyll conductance g_M, is used to calculate C_M, which is iterated. Temperature dependence is simulated with empirical functions (Note S8, Table S2). For each combination of inputs, the locality of Rubisco between BS and M ($\chi_{Rubisco}$) together with the rate of flow through CEF (f_{Cyc}) were fitted to maximise *A*. This resulted in light reactions generating exactly the ATP and NADPH which was consumed by dark reactions, while the ATP–limited model and the NADPH–limited models converged to output the same level of *A*. The outputs of these submodels (V_{OBS}, V_{CBS}, V_{OM}, and V_{CM}) were inputted to a generalised stoichiometric model of assimilation (Bellasio, 2017), used to calculate reaction rates, and fluxes across the BS and M interface (Figure S1). Here, three additional inputs partition key processes between the BS and M: f_{PR}, for phosphoglycerate reduction; f_{CS}, for carbohydrate synthesis; f_{PPDK}, for pyruvate phosphate dikinase (Table 1). Model parameterisation and sensitivity are described in Notes S9 (coefficients are in Table S3) and S10, respectively.

Plants, gas exchange, and fluorometry

Plants of *Oryza sativa* subsp. *indica*, modern, high–yielding variety Takanari (Taylaran *et al.*, 2009) were germinated and grown in 1.5 L pots filled with Martins potting mix (80% composted bark, 10% coir, 10% sand, complete fertiliser), in acrylate greenhouses located in Canberra (35°S, 149°E) under natural illumination in April – May 2018. Pots were partially submerged for a third of the depth in polypropylene tubs and watered weekly for six weeks. Gas exchange and fluorescence were measured on a fully expanded leaf with a setup similar to Bellasio and Griffiths (2014b). Briefly, a portable gas exchange system (LI6400XT, Li–Cor, Lincoln, USA) was modified to operate at low CO_2 concentrations (see licor.com) and fitted with a 6400–06 PAM2000 adapter, holding a fibre probe in the upper leaf cuvette distant enough to avoid shading. Light was provided by a bespoke red–blue light source, positioned to illuminate uniformly the leaf. Light intensity was measured through an in–chamber Gallium arsenide photodiode, calibrated using a Li–250 light

sensor (Li–Cor). Neoprene gaskets were used on both sides of the cuvette. A mixture of 2 % O_2 was prepared by mixing ambient air and N_2 with a bespoke gas mixing unit (kindly assembled by Suan Chin Wong). This mix or ambient air was CO_2–scrubbed with soda lime and humidified to a dew point of 15–17 °C upstream of the inlet to maintain water vapour pressure deficit around 1 kPa. CO_2 was added from a cylinder (Isi, Vienna, Austria), using the CO_2 injection unit of the LI6400XT. PSII yield was measured with a Dual PAM–F (Heinz Walz GmbH, Effeltrich, Germany). Pulse intensity was adjusted to be between 10,000 and 12,000 µmol m^{-2} s^{-1} thereby exceeding the requirements of between 6,000 and 8,000 µmol m^{-2} s^{-1}, depending on CO_2 and *PPFD* levels, to saturate the fluorescence signal. Mass flow leaks (Boesgaard *et al.*, 2013) were monitored with a gas flow meter as detailed in Bellasio, C. *et al.* (2016), and sealed with a tiny ridge of atoxic gelatine laid between the gaskets and the leaf. Four photosynthetic response curves were measured at 25 °C on *n*=4 plants as detailed in Bellasio, C. *et al.* (2016). A/C_i curves were measured under a *PPFD* of 1200 µmol m^{-2} s^{-1}, light curves were measured under a C_a of 420 µmol mol^{-1}. Flow rate was 490 µmol s^{-1}; CO_2 diffusion through the gaskets was compensated by lengthening the tubing of the LI6400XT reference gas.

Results

Gas exchange

The operational conditions of rice plants were characterised by a comprehensive gas exchange experiment, which combined measurements under ambient and low O_2. Primary, diffusion leak–corrected data appear as symbols in Figure 2, PSII yield is shown in Figure S3. Overall, rice displayed typical C_3 responses. Under high *PPFD* (Figure 2A), *A* was lower under ambient O_2 (closed symbols) than under low O_2 (open symbols) because of photorespiration. The quantum yield for assimilation (the initial slope of the curves), was higher under low O_2 (0.0397±0.0002 and 0.0512±0.0023 under ambient and low O_2, respectively). Under low C_i (Figure 2B), *A* was higher under low O_2 than under ambient O_2 because of O_2 competitive inhibition of Rubisco. Assimilation saturated at relatively lower C_i under low O_2 (open symbols) than under ambient O_2. The stomatal conductance (g_S) measured in *A*/*PPFD* curves (Figure 2C) increased monotonically with *PPFD* showing a saturating response similar to that of the *A*/*PPFD* curve. Under varying external CO_2 concentration (C_a), g_S decreased non–linearly with slope depending on the O_2 level. Rice had a slightly higher *in vivo* $S_{C/O}$ (Table 1) than that found *in vitro* (Hermida-Carrera *et al.*, 2016) perhaps for the tight association between mitochondria and chloroplasts that evolved to maximise photorespiratory CO_2 recapture (Sage & Sage, 2009; Hatakeyama & Ueno, 2016). Under a *PPFD* of 500 µmol m^{-2} s^{-1}, rice operated at a relatively low V_O/V_C of circa 0.3 [Figure S4, compare with Bellasio *et al.* (2014)].

Simulating assimilation and stomatal conductance of native C_3 rice

206 *A/C*$_i$ and *A/PPFD* curves responses for rice were simulated in the same conditions used for gas
207 exchange measurements. The model predicted with accuracy *A/PPFD* (Figure 2A) and *A/C*$_i$ curves
208 (Figure 2B) measured under ambient O_2, but overestimated *A/PPFD* and *A/C*$_i$ curves under low O_2
209 and high C_a. We attribute this to triose phosphate limitation, and to the feedbacks regulating the
210 electron transport chain through the quenching of *Y(II)* under low O_2 (Figure S3) which we have
211 addressed in Bellasio (2018) but not considered in this model, for simplicity. The simulated
212 stomatal behaviour captures very well the shape of the stomatal response, in both *A/PPFD* and *A/C*$_i$
213 curves and at both O_2 levels.

214 *Simulating gas exchange of C_2, C_2+C_4 and C_4 rice*

215 Here, simulations were intended to capture hypothetical best–case scenario, assuming unlimited
216 phenotypic plasticity whereby Rubisco is optimally distributed and electron transport processes
217 fully accommodate CEF and NDH levels. Conditions and fitting routines were the same as used for
218 the C_3 simulations. The C_2 shuttle and progressive levels of C_4 activity were introduced in native
219 rice by manipulating the activity of PEPC (through the inputs V_{PMAX} and $V_{P(J)}$), the locality of GDC
220 (ξ_{GDC}), the engagement of the NDH pathway of electron transport (f_{NDH}) and the BS apportioning of
221 light respiration (f_{RLIGHT}, see Table 1 for full details). The levels of the fitted inputs $\chi_{Rubisco}$ and f_{Cyc}
222 are shown in Figure S5. These are relevant for bioengineering as they indicate the required physical
223 distribution of Rubisco, and the necessary adjustments to the electron transport chain. *A/PPFD*
224 curves (Figure 3A) simulated at a C_a of 400 µmol mol^{-1} intersect around a *PPFD* of 300 µmol m^{-2} s^{-1}.
225 Under lower *PPFD*s C_2 *A* was the highest and C_4 was the lowest. Under higher *PPFD*s *A*
226 increased proportionally with the level of CCM engagement and was ~22% higher for C_4 than C_3 at
227 a *PPFD* of 1500 µmol m^{-2} s^{-1}. The analysis of *A/C*i curves (Figure 3B) revealed expected
228 differences in predicted gas change characteristics between photosynthetic types, with *A* at C_a lower
229 than ~550 µmol mol^{-1} being progressively higher for plants operating CCMs at increasing
230 engagement. But the operation of a CCM necessarily sacrifices *A* under higher C_a. There were
231 striking differences in stomatal conductance, which was around 40% less in C_4 than in C_3 under a
232 *PPFD* of 1500 µmol m^{-2} s^{-1} and a C_a of 400 µmol mol^{-1} (Figure 3C), indicating that the same level
233 of *A* was achieved with lower transpiration and higher water use efficiency, in line with differences
234 between extant C_3 and C_4 species (Bellasio *et al.*, 2018; Quirk *et al.*, 2018) although in the field
235 there is some negative feedback on the effect on WUE because of temperature changes. The same
236 differences were maintained in the simulated *A/C*i curves (Figure 3D). Notably these differences in
237 g_S resulted solely from biochemical differences between photosynthetic types (sensed by the
238 quantity τ) while all other parameters were maintained at C_3 levels. The operation of the CCMs
239 resulted in an increase in the CO_2 concentration in the BS (Figure 3E and 3F) and in the consequent
240 reduction of the ratio between Rubisco oxygenation and carboxylation (Figure 3G and 3H). The
241 output fraction of BS Rubisco carboxylation V_{CBS}/V_C, which depends both on C_{BS} and on $\chi_{Rubisco}$, is

shown in Figure 3I and 3J. V_{CBS}/V_C was relatively invariant with *PPFD* in all photosynthetic types except C_4, where it slightly decreased below 500 µmol m^{-2} s^{-1} (Figure 3I). In *A/Ci* curves V_{CBS}/V_C increased at low C_a for C_2 and C_2+C_4 types and decreased at high C_a for the C_4 type. Leakiness (the rate of CO_2 retrodiffusion from the BS relative to PEP carboxylation rate), of relevance for isotopic studies, (Cernusak *et al.*, 2013; Bellasio & Griffiths, 2014b) is plotted in Figure S6. To isolate any effect of CO_2 diffusion through the mesophyll and stomata, these simulations were repeated using C_M as input, and are shown in Figure S7.

Assimilatory gain/loss of C_2, C_2+C_4 and C_4 rice at different temperatures, C_a, and PPFD

This set of simulations explored gains and losses of operating different types of photosynthesis, as compared to C_3. Three scenarios were simulated: one of unlimited plasticity of the electron transport chain and two in which some elements of the electron transport chain remain in a C_3 configuration. In the best case scenario electron transport processes fully accommodate the ATP demand of different types of CCM through the optimisation of the levels of CEF (f_{Cyc}) and by allowing expression of the NDH complex in C_2+C_4 and C_4 types (f_{NDH}>0). Figure 4 shows that operating C_2 was beneficial at all temperatures and *PPFD*s, but gains were generally lower than 10% (Figure 4B), as compared to C_3 (Figure 4A). Operating C_2+C_4 was slightly counterproductive below a *PPFD* of 450 µmol m^{-2} s^{-1} and a temperature of 40° C but allowed substantial gains above (Figure 4C). The range in which operating C_4 photosynthesis did not confer net benefits was cutting diagonally below a temperature of 40° C and a *PPFD* of 500 µmol m^{-2} s^{-1} (Figure 4D). The possible gains and losses were much more pronounced for C_4 than for C_2 and C_2+C_4 types. In the operation of the C_4 cycle most of the energy saved by suppressing photorespiration is consumed by the regeneration of PEP; the resulting balance depends on their relative flux, and can be quantified through the quantum efficiency of assimilation *Y(CO_2)*, shown on incident light basis in Figure S8. *Y(CO_2)* was very similar for C_3 and C_2 types. C_2+C_4 and C_4 had higher *Y(CO_2)* than C_3 at high *PPFD*s, but lower at low *PPFD*s. Overall, *Y(CO_2)* was slightly lower than our previous measurements in tobacco and maize (Bellasio, C. *et al.*, 2016; Bellasio, Chandra *et al.*, 2016), which we attribute to slightly lower $Y(II)_{LL}$ and *s* (Table 1).

We then compared CCM types to C_3 assimilation in the temperature and C_a space, under a moderate *PPFD* of 700 µmol m^{-2} s^{-1}, meant to capture illumination of an ordinary erect leaf of a modern cultivar in the upper level of the canopy, in the same optimistic scenario of variable CEF and engaged NDH (Figure 4E). C_2 assimilation was beneficial at all temperatures and C_a (Figure 4F). Gains were greater than 10% in a relatively broad set of conditions including under ambient C_a at high temperatures. The C_4 and C_2+C_4 types were disadvantageous above a C_a of around 450 µmol mol^{-1} and below 40 °C – a broader range than under higher *PPFD* (Figure 3B). The C_4 and C_2+C_4 types were progressively more advantageous at higher temperature and low C_a.

Similar simulations were carried out to represent a less optimistic scenario whereby the activity of the NDH complex remained at C_3 levels (f_{NDH}=0) for all photosynthetic types (Figure 5, top row). The marginal gains were maintained for the C_2 type (Figure 5A); however, C_2+C_4 and C_4 types were counterproductive in a broader range of *PPFD*s roughly cutting below a *PPFD* of 700 μmol m^{-2} s^{-1} for the C_2+C_4 type and 900 μmol m^{-2} s^{-1} for the C_4 type (Figure 5B and 5C).

In a pessimistic scenario, in addition to the incapacity to express sufficient NDH complex (f_{NDH}=0), CCM types were unable to modify the flux through CEF, which remained capped at C_3 levels (Figure 5, bottom row). Here, the marginal gains were maintained for C_2 photosynthesis (Figure 5D); however, the C_2+C_4 type was counterproductive below a *PPFD* of 1000 μmol m^{-2} s^{-1}, while the C_4 type was counterproductive at all *PPFD*s below a temperature of 30°C (Figure 5E and 5F). Severe losses in excess of 40% were predicted for the C_4 type at ordinary temperatures and moderate to low *PPFD*s.

Metabolite transport

Two further sets of simulations estimated the metabolite fluxes between the M and the BS by manipulating the level of C_4 engagement through increasing levels of V_P (Figure 6) so as to represent the full C_2+C_4 continuum from C_2 (left of each panel) to C_4 (right of each panel). In a first scenario (Figure 6A), the level of ATP demand in the BS was minimised. In these conditions, phosphoglycerate is not reduced in the BS but diffuses to the M and is reduced therein to dihydroxyacetone phosphate, DHAP. A minimal part of DHAP is used by carbohydrate synthesis, but the majority diffuses back to BS to replenish the sugar phosphates pool. This drives the metabolite exchange between the M and the BS to a maximum. In addition, because phosphoglycerate reduction is the main NADPH sink in the BS, when ATP demand in the BS is minimal, the NADPH demand in the BS is also minimal. This requires by–passing the malate dehydrogenase in the M, and, to maintain the efficiency of the CCM despite the inability to operate the malate shuttle, the CCM works through alanine and aspartate (Bellasio, 2017). This condition is suboptimal because it requires high concentration gradients of aspartate and alanine when malate and pyruvate do not transport CO_2 (Arrivault *et al.*, 2017). At low levels of C_4 engagement, when V_P was low, glycine and serine were operating the C_2 shuttle. The model predicts that the reducing power generated in the BS by the decarboxylation of glycine, which could not be used by phosphoglycerate reduction because of the insufficient ATP availability, was returned to the M by the malate and pyruvate shuttle in a 'backward' C_4 cycle. As V_P increased, the flux of glycine and strength of the C_2 cycle [which scales with V_P, see details in Bellasio (2017)] was progressively reduced, diminishing the excess NADPH in BS together with the malate and pyruvate fluxes that decrease to zero with V_P. With the increase in V_P, the fitted fraction of Rubisco carboxylation in BS increased linearly, causing the ratio of ATP demand in BS relative to M to increase linearly (Figure 6C).

An opposite scenario, where fluxes were minimal, was simulated by fitting f_{PR} and f_{CS} to minimise the sum of squared flow rates between BS and M (Figure 6B). In these conditions the increase of phosphoglycerate reduction in the BS drove the ATP demand in the BS to a maximum (Figure 6D). The total fluxes were less than half those of the previous case (54 *versus* 130 μmol m^{-2} s^{-1}); the main metabolites to be transported in these conditions were malate and pyruvate, which were the sole compounds to support the CCM while the flux of aminoacids was minimal. Despite the malate and pyruvate shuttle working in full, and exporting reducing power from the M to the BS, the NADPH demand in the BS was high (Figure 6D), requiring substantial linear electron flow in the BS (~18 μmol m^{-2} s^{-1} of NADPH).

Discussion

This work set out to study the theoretical underpinnings of the introduction of CCMs into C_3 metabolism. A model of enzyme and light–limited assimilation was newly derived to account for the stoichiometry of Bellasio (2017) (Table S1) augmented to include the explicit mechanistic description of the electron transport chain (Bellasio, 2018), and a hydromechanical and biochemical model of stomatal conductance recently shown to work for C_3 and C_4 plants (Bellasio *et al.*, 2017). We shall stress four points distinguishing the importance of this work. Firstly, by including a hydromechanical submodel we provide a means to connect plant assimilatory biochemistry to plant hydraulics, allowing the concurrent investigation of photosynthesis and water use. Secondly, this is the only study comparing C_2 performance with C_3, C_2+C_4 and C_4 seamlessly within a single model, offering a further improvement over approaches targeted to specific types. Thirdly, this is the only study estimating the metabolite fluxes necessary to operate the different photosynthetic types. Lastly, the model marries biochemically comprehensiveness (it includes all main reactions of the photosynthetic metabolism) with computational speed, required by larger scale modelling. This model is generally applicable, and will be valuable for ecophysiological and evolutionary studies, but we will address evolution at a later stage. Here, we applied the modelling framework to predict assimilation and metabolite fluxes in a three dimensional environmental landscape (t × C_a × *PPFD*) using parameters derived for rice. Next, we make some general considerations on the introduction of a CCM in C_3 metabolism, and we elaborate on the special case of rice.

There is a pervasive belief that the introduction of C_4 photosynthesis into C_3 plants will unconditionally increase assimilation, supported by models based on the assumption that ATP and NADPH are unlimited (Heckmann *et al.*, 2013). However, decades of comparison between C_4 and C_3 plants have shown that C_3 plants may be advantaged in a range of conditions [e.g. (Ehleringer *et al.*, 1997; Ghannoum *et al.*, 2000; Christin & Osborne, 2014)]. We showed that, when energy budgets were accounted for, C_4 photosynthesis becomes unfavourable at high CO_2 concentrations, low *PPFD* and low temperatures, and therefore provide a novel theoretical framework to explain such experimental observations.

Bundle sheath permeability mediates trade–offs imposed by light intensity

Modern crops like rice have typically a LAI (leaf area per ground area) of 5–6, meaning that the majority of leaves are shaded and, importantly, the overall performance of C_4 types will compromise full–light advantages and shade disadvantages. The key parameter governing photosynthetic losses under low *PPFD* in C_4 photosynthesis is BS conductance, g_{BS} (Bellasio & Griffiths, 2014b). g_{BS} controls the flux of CO_2 released in the BS that retrodiffuses to the M, called leakage (Farquhar, 1983). g_{BS} can vary several orders of magnitude in nature and can affect A substantially (Kromdijk *et al.*, 2014; Yin & Struik, 2017), in particular at high levels of CCM engagement (Figure S9). Under high temperature, g_{BS} is reported to increase (Yin *et al.*, 2016), while under low *PPFD* V_P decreases, driven by a reduced rate of ATP production (Bellasio & Griffiths, 2014b). In these conditions, leakage reduces C_{BS}, and, in C_4 plants, it dissipates energy through the ATP–dependent regeneration of phospho*enol*pyruvate required to re–fix the leaked CO_2, making the CCM counterproductive (Tazoe *et al.*, 2008; Ubierna *et al.*, 2011; Ubierna *et al.*, 2013; Bellasio & Griffiths, 2014b; Sun *et al.*, 2014; Pignon *et al.*, 2017). In nature, plants minimise the ratio between leakage and metabolite fluxes by preferentially localising plasmodesmata at the interface between M and BS, while apoplastic diffusion is often reduced by the deposition of a gas–tight suberized cell wall (Sowinski *et al.*, 2008; Sowiński, 2013; Danila *et al.*, 2016; Danila *et al.*, 2018). If low g_{BS} may therefore appear desirable (though perhaps difficult to achieve), high symplastic permeability is required to sustain metabolite diffusion [Figure 6, (Weber & von Caemmerer, 2010)], and this dilemma constitutes an efficiency trade–off that is inherent to the C_4 CCM – and unavoidable (Bellasio & Griffiths, 2014a). Indeed, to attune leakage to *PPFD* levels, g_{BS} in maize was found to adjust during growth (Bellasio & Griffiths, 2014b) as well as in adult leaves (Bellasio & Griffiths, 2014a).

Future CO_2 levels

Rising anthropogenic atmospheric CO_2 concentrations will favour C_3 assimilation over C_4. Apart from the difficulties in predicting future CO_2 levels – not addressed here – predicting assimilation under changing CO_2 is very difficult. When plants are exposed to a high CO_2 level for a long time they may downregulate the pool of Rubisco and PEPC (Ghannoum *et al.*, 2000; Leakey *et al.*, 2004; Long *et al.*, 2006; Leakey *et al.*, 2012), at the same time, producing fewer stomata (Way *et al.*, 2011; Franks *et al.*, 2012)(Quirk, Bellasio and Beerling, Annals of Botany, *in press*.). There is a growing body of data gained under controlled conditions [e.g. (Bellasio *et al.*, 2018; Quirk *et al.*, 2018)] and in free air experiments [e.g. (Bishop *et al.*, 2015)], yet, responses are species specific and, currently, evidence is not sufficient to generalise acclimation responses of C_4 and C_3 plants. As a result, it is common practice in climate modelling to take assimilatory responses measured under transient changes in CO_2 levels (A/C_a curves) as predictive of stable responses of plants grown under different CO_2 levels, that is, no large scale models include representation of the physiological

acclimation to future CO_2 level (Rogers *et al.*, 2017). With this principle, using simple interpolation of the best case scenario shown in Figure 4H, at 25 °C, C_4 assimilation would equal C_3 assimilation at a C_a of 465 µmol mol^{-1}, a level that would be exceeded in 2036 according to the A2 scenario of carbon emission mitigation (http://www.ipcc-data.org/observ/ddc_co2.html).

Strategies for engineering a CCM

In the face of global warming, the introduction of CCMs in a C_3 crop such as rice was proposed as a possible strategy to increase yield (Leegood, 2013; Long *et al.*, 2015). An operational C_2 shuttle was considered as a first step in bio–engineering, with the final goal of obtaining a fully expressed C_4 type. Of the three biochemical C_4 subtypes (NADP–ME, NAD–ME, PEPCK), the NADP–ME was chosen as the initial target (Kajala *et al.*, 2011), as it is operated by the crops with greatest productivity (Furbank, 2011) and would require introducing a smaller number of enzymes [in M cells carbonic anhydrase, PEPC, malate dehydrogenase, and pyruvate–phosphate dikinase; in BS cells NADP–ME, plus eight transmembrane transporters (Kajala *et al.*, 2011)]. Other subtypes require additional enzymes [aspartate and alanine aminotransferase, PEPCK, NAD–ME (Wang *et al.*, 2014), plus up to three transporters (Schlüter *et al.*)] and were not considered here, but see Bellasio (2017). Traditionally, strategies for engineering a CCM have emphasized the manipulation of dark reactions and the associated genetics (Kajala *et al.*, 2011; Leegood, 2013). Here we point to two overlooked factors required for the operation of a CCM, namely anatomy and light reactions.

Firstly, leaf anatomy needs to be adjusted depending on the level of C_4 cycle expression. Anatomy and biochemistry of the BS are mutually interdependent (Bellasio & Griffiths, 2014c). The requirement in light harvesting optical cross section depends on the ATP demand, and determines the required BS volume, mediated by the size of the ATP–generating light harvesting machinery, plus the volume of the dark reactions machinery (Bellasio & Lundgren, 2016). Minimal ATP demand in the BS may be desirable as it would require the smallest BS, and therefore require minimum modification of the current rice anatomy, but would lead to the unwanted necessity of high gradients and flux rates, and require the expression of high levels of metabolite transporters (Pick *et al.*, 2011). Aiming at a high ATP demand would have the benefit of requiring the minimum expression of transporters but would require the largest electron transport chain, and therefore a more radical modification of the native C_3 anatomy. Identifying a desired anatomical target requires therefore first to identify a biochemical ideotype. Each of the two extreme solutions shown in Figure 6 would entail limited operational robustness (Pick *et al.*, 2011), as there would not be any freedom to accommodate transient environmental change (Bellasio & Griffiths, 2014c). A ‘robust flexibility’ would be positioned half–way between these two opposite scenarios, for instance where the ATP demand in the BS relative to M is 0.7. The potential ratio of ATP production in the BS relative to M must exceed 0.7 by a considerable safety margin (Bellasio & Lundgren, 2016) to counter changing light conditions (Bellasio & Griffiths, 2014c). To achieve this, the light absorbed

in the BS relative to M under white light, must be close to 0.7. Currently, the size and pigmentation of rice BS is insufficient (Bellasio & Lundgren, 2016). A suitable situation was found in maize, which had a BS pigmentation circa twice that of the M, and allocated ~30% of the total leaf section area to the BS (Bellasio & Lundgren, 2016) and should be considered as the target for C_4 rice. Further, reaching the required levels for g_{BS} will require engineering the appropriate density of plasmodesmata (Danila *et al.*, 2016), reducing leakage, and possibly allow for acclimation of g_{BS} during growth (see above). Alternatively, higher efficiency could be reached by operating the C_4 cycle only in those parts of the canopy where the *PPFD* is higher than a given threshold, but this seems difficult to achieve also because it is adopted neither in mature nor in developing maize leaves (Wang *et al.*, 2013).

Secondly, the operation of a C_4 cycle will require important modifications to the electron transport chains. We showed that when cyclic electron flow, CEF (f_{Cyc}) and the NDH pathway (f_{NDH}) were allowed to vary (Figure 4), the performance of C_2+C_4 and C_4 types was maximal. This optimal scenario reflects the idea that electron transport processes may spontaneously adjust in response to the expression of a CCM, responding to an increase in ATP demand, through flexibility mechanisms inherent in native chloroplasts (Takeuchi *et al.*, 2000). Higher levels of f_{NDH} would benefit C_4 assimilation, but may be physiologically implausible, for example because NDH is very expensive to produce and maintain. It is possible, however, that rice does not have the potential to express adequate level of CEF and NDH components. If f_{NDH} is capped at C_3 levels the performance of C_4 rice will be lower (Figure 5 A–C), and if f_{Cyc} is capped at C_3 levels A would be depressed even further (Figure 5 D–F).

Considering the complexities and trade–offs of implementing a C_4 cycle, C_2 rice may be a desirable product of bioengineering efforts. Despite the relative operational simplicity, the engagement of a C_2 shuttle always increased assimilation rate, relative to C_3. The assimilation gain was relatively small under ambient C_a, but increased with temperature at low C_a (Figure 4F). Although in water–rich rice paddies plants can maintain stomata open and extreme photorespiratory conditions might not occur at mid–latitudes (where temperatures are milder and the subsp. *japonica* is favoured), they may occur at low–latitudes (where temperatures are higher and the subsp. *indica* is favoured), and, particularly, for dryland rice, which would probably be the crop to benefit most from the introduction of a C_2 CCM. In the simulations, the locality of Rubisco activity, as $\chi_{Rubisco}$, was adjusted continuously at varying C_M always resulting in optimal Rubisco activity. In nature, however, the proportion of Rubisco in the BS may change only on evolutionary timescales and may be plant–specific. Consequently, there may be a trade–off between optimisation for photorespiratory conditions, by compartmentalising more Rubisco to the BS, or for non–photorespiratory conditions by allowing all Rubisco in the M, with easier access to intercellular CO_2. Allocating 10 % of Rubisco in the BS was a good compromise (Figure S5).

From leaf–level to crop

Upscaling these findings to calculate crop yield will be a challenging task. Firstly, it will require modelling of the canopy light environment (Song *et al.*, 2013), possibly including diel light cycles of fully illuminated leaves (Wu *et al.*, 2017) and the transient illumination in shaded leaves (Pearcy *et al.*, 1997), nitrogen allocation (Buckley *et al.*, 2002; Dewar *et al.*, 2012), the effect of different canopy architectures (Burgess *et al.*, 2017), the response of A and g_S to temperature and humidity (Yin & Struik, 2017). Ideally, the description could consider the potential losses due to suboptimal stomatal aperture (Vialet-Chabrand *et al.*, 2016; Bellasio *et al.*, 2017), and the mid–morning depressions of photosynthetic capacity (Horton & Murchie, 2000). The necessity of translating assimilation into grain yield will add further complexities and require a dedicated crop model accounting for root growth, nitrogen uptake, pathogens, as well as the interactions between cultivars and climate (Li *et al.*, 2015; Paleari *et al.*, 2017). There is an urgent need for addressing some of these challenges. This model offers the necessary underpinnings and can be readily used as a submodel for modelling assimilation at higher spatial level.

Conclusion

We developed new ATP–limited, and NADPH–limited submodels of assimilation, as well as a light reaction submodel, coupled with a stomatal submodel. The resulting model connects light harvesting to dark assimilatory biochemistry and hydraulics and is valid for any photosynthetic type. The equations were solved analytically and will be valuable for evolutionary as well as ecophysiological studies, and we encourage their use also for larger scale modelling. The model was calibrated and tested on primary gas exchange and fluorescence data measured on rice. By simulating the introduction of CCMs in C_3 metabolism we showed that C_4 photosynthesis becomes disadvantageous under a set of environmental conditions (low light, low temperatures and high CO_2) thus providing theoretical support for decades of ecophysiological observations. For the expression of a CCM to be advantageous, any modifications to dark reactions need to be accompanied by substantial modifications to light reactions. Specifically, engineering an appropriate electron transport chain, with the possibility of expressing the NDH complex and adjusting levels of cyclic electron flow will be required. These will also need to be accompanied by anatomical modifications to accommodate the biochemical and light harvesting machinery and by the expression of suitable levels of transporters to allow adequate metabolite traffic.

Acknowledgments

We are grateful to Ross Deans, Joe Quirk, Florian Busch, and Pascal–Antoine Christin for review, to Alexis Moschopoulos, Emily Beardon, Yuzhen Fan, and Deyun Qiu for plants, to Rosario Maggistro for help, to Dean Price for the fluorometer, to Susanne von Caemmerer and Suan

Chin Wong for gas exchange equipment, to Tom Sharkey for initially suggesting to apply the model to the introduction of the C_4 cycle in rice. CB gratefully acknowledges funding through a H2020 Marie Skłodowska–Curie individual fellowship (DILIPHO, ID: 702755). GDF gratefully acknowledges the ARC Centre of Excellence for Translational Photosynthesis (Grant number CE140100015).

This work was solely driven by the Authors' curiosity, is not part of – and is not funded by – projects aimed at creating C_4 rice; the Authors have no conflict of interest.

Author Contributions

CB conceived of the research, performed measurements, developed and coded the models, ran simulations. CB and GDF wrote the paper.

Availability

The model, coded in Excel, is made freely available in Supporting Information. The model does not include 'live' scripts and is fully operational in the open access suite 'Apache Open Office'.

References

Arrivault S, Obata T, Szecówka M, Mengin V, Guenther M, Hoehne M, Fernie AR, Stitt M. 2017. Metabolite pools and carbon flow during C_4 photosynthesis in maize: $^{13}CO_2$ labeling kinetics and cell type fractionation. *Journal of Experimental Botany* **68**(2): 283-298.

Atkinson RRL, Mockford EJ, Bennett C, Christin P-A, Spriggs EL, Freckleton RP, Thompson K, Rees M, Osborne CP. 2016. C_4 photosynthesis boosts growth by altering physiology, allocation and size. *Nature Plants* **2**: 16038.

Bellasio C. 2017. A generalised stoichiometric model of C_3, C_2, C_2+C_4, and C_4 photosynthetic metabolism. *Journal of Experimental Botany* **68**(2): 269-282.

Bellasio C. 2018. A generalised dynamic model of leaf-level C_3 photosynthesis combining light and dark reactions with stomatal behaviour. *Photosynthesis Research* **10.1007/s11120-018-0601-1**.

Bellasio C, Beerling DJ, Griffiths H. 2016. Deriving C_4 photosynthetic parameters from combined gas exchange and chlorophyll fluorescence using an Excel tool: theory and practice. *Plant, Cell & Environment* **39**(6): 1164-1179.

Bellasio C, Beerling DJ, Griffiths H. 2016. An Excel tool for deriving key photosynthetic parameters from combined gas exchange and chlorophyll fluorescence: theory and practice. *Plant Cell and Environment* **39**(6): 1180–1197.

Bellasio C, Burgess SJ, Griffiths H, Hibberd JM. 2014. A high throughput gas exchange screen for determining rates of photorespiration or regulation of C4 activity. *Journal of Experimental Botany* **65**(13): 3769-3779.

Bellasio C, Griffiths H. 2014a. Acclimation of C4 metabolism to low light in mature maize leaves could limit energetic losses during progressive shading in a crop canopy. *Journal of Experimental Botany* **65**(13): 3725-3736.

Bellasio C, Griffiths H. 2014b. Acclimation to Low Light by C_4 maize: Implications for Bundle Sheath Leakiness. *Plant Cell and Environment* **37**(5): 1046-1058.

Bellasio C, Griffiths H. 2014c. The operation of two decarboxylases (NADPME and PEPCK), transamination and partitioning of C4 metabolic processes between mesophyll and bundle sheath cells allows light capture to be balanced for the maize C4 pathway. *Plant Physiology* **164**: 466-480.

Bellasio C, Lundgren MR. 2016. Anatomical constraints to C_4 evolution: light harvesting capacity in the bundle sheath. *New Phytologist* **212**(2): 485–496.

Bellasio C, Quirk J, Beerling DJ. 2018. Stomatal and non-stomatal limitations in savanna trees and C_4 grasses grown at low, ambient and high atmospheric CO_2. *Plant Science* **274**: 181-192.

Bellasio C, Quirk J, Buckley TN, Beerling D. 2017. A dynamic hydro-mechanical and biochemical model of stomatal conductance for C4 photosynthesis. *Plant Physiology*.

Bishop KA, Betzelberger AM, Long SP, Ainsworth EA. 2015. Is there potential to adapt soybean (Glycine max Merr.) to future [CO_2]? An analysis of the yield response of 18 genotypes in free-air CO_2 enrichment. *Plant, Cell & Environment* **38**(9): 1765-1774.

Boesgaard KS, Mikkelsen TN, Ro-Poulsen H, Ibrom A. 2013. Reduction of molecular gas diffusion through gaskets in leaf gas exchange cuvettes by leaf-mediated pores. *Plant, Cell & Environment* **36**(7): 1352-1362.

Buckley TN, Adams MA. 2011. An analytical model of non-photorespiratory CO_2 release in the light and dark in leaves of C_3 species based on stoichiometric flux balance. *Plant, Cell & Environment* **34**(1): 89-112.

Buckley TN, Miller JM, Farquhar GD. 2002. The mathematics of linked optimisation for water and nitrogen use in a canopy. *Silva Fennica* **36**(3): 639-669.

Buckley TN, Sack L, Farquhar GD. 2016. Optimal plant water economy. *Plant, Cell & Environment* **40**(6): 881-896.

Burgess AJ, Retkute R, Herman T, Murchie EH. 2017. Exploring Relationships between Canopy Architecture, Light Distribution, and Photosynthesis in Contrasting Rice Genotypes Using 3D Canopy Reconstruction. *Frontiers in Plant Science* **8**: 734.

Busch FA, Sage RF. 2017. The sensitivity of photosynthesis to O_2 and CO_2 concentration identifies strong Rubisco control above the thermal optimum. *New Phytologist* **213**(3): 1036-1051.

Busch FA, Sage RF, Farquhar GD. 2018. Plants increase CO_2 uptake by assimilating nitrogen via the photorespiratory pathway. *Nature Plants* **4**: 46–54

Cernusak LA, Ubierna N, Winter K, Holtum JAM, Marshall JD, Farquhar GD. 2013. Environmental and physiological determinants of carbon isotope discrimination in terrestrial plants. *New Phytologist* **200**: 950-965.

Christin PA, Osborne CP. 2014. The evolutionary ecology of C_4 plants. *New Phytologist* **204**(4): 765-781.

Covshoff S, Szecowka M, Hughes TE, Smith-Unna R, Kelly S, Bailey KJ, Sage TL, Pachebat JA, Leegood R, Hibberd JM. 2016. C_4 Photosynthesis in the Rice Paddy: Insights from the Noxious Weed Echinochloa glabrescens. *Plant Physiology* **170**(1): 57-73.

Danila F, Quick WP, White RG, Furbank RT, von Caemmerer S. 2016. The Metabolite Pathway between Bundle Sheath and Mesophyll: Quantification of Plasmodesmata in Leaves of C_3 and C_4 Monocots. *The Plant Cell* **28**(6): 1461-1471.

Danila FR, Quick WP, White RG, Kelly S, von Caemmerer S, Furbank RT. 2018. Multiple mechanisms for enhanced plasmodesmata density in disparate subtypes of C_4 grasses. *Journal of Experimental Botany* **69**(5): 1135-1145.

Dewar RC, Tarvainen L, Parker K, Wallin G, McMurtrie RE. 2012. Why does leaf nitrogen decline within tree canopies less rapidly than light? An explanation from optimization subject to a lower bound on leaf mass per area. *Tree Physiology* **32**(5): 520-534.

Ehleringer JR, Cerling TE, Helliker BR. 1997. C4 photosynthesis, atmospheric CO_2, and climate. *Oecologia* **112**(3): 285-299.

Evans JR, von Caemmerer S, Vogelmann TC 2007. Balancing light capture with distributed metabolic demand during C_4 photosynthesis. In: J.E. Sheehy, P.L. Mitchell, B. Hardy eds. *Charting new pathways to C_4 rice*: IRRI International Rice Research Institute. Word scientific pubishing, Singapore.

Farquhar G, Wong S. 1984. An empirical model of stomatal conductance. *Functional Plant Biology* **11**(3): 191-210.

Farquhar GD. 1983. On the Nature of Carbon Isotope Discrimination in C_4 Species. *Australian Journal of Plant Physiology* **10**(2): 205-226.

Franks PJ, Leitch IJ, Ruszala EM, Hetherington AM, Beerling DJ. 2012. Physiological framework for adaptation of stomata to CO_2 from glacial to future concentrations. *Philosophical Transactions of the Royal Society B-Biological Sciences* **367**(1588): 537-546.

Friso G, Majeran W, Huang MS, Sun Q, van Wijk KJ. 2010. Reconstruction of Metabolic Pathways, Protein Expression, and Homeostasis Machineries across Maize Bundle Sheath and Mesophyll Chloroplasts: Large-Scale Quantitative Proteomics Using the First Maize Genome Assembly. *Plant Physiology* **152**(3): 1219-1250.

Furbank RT. 2011. Evolution of the C_4 photosynthetic mechanism: are there really three C4 acid decarboxylation types? *Journal of Experimental Botany* **62**(9): 3103-3108.

Galmés J, Hermida-Carrera C, Laanisto L, Niinemets Ü. 2016. A compendium of temperature responses of Rubisco kinetic traits: variability among and within photosynthetic groups and impacts on photosynthesis modeling. *Journal of Experimental Botany* **67**(17): 5067-5091.

Ghannoum O, Caemmerer SV, Ziska LH, Conroy JP. 2000. The growth response of C_4 plants to rising atmospheric CO_2 partial pressure: a reassessment. *Plant, Cell & Environment* **23**(9): 931-942.

Gowik U, Bräutigam A, Weber KL, Weber APM, Westhoff P. 2011. Evolution of C_4 Photosynthesis in the Genus Flaveria: How Many and Which Genes Does It Take to Make C_4? *The Plant Cell Online* **23**(6): 2087-2105.

Hahn A, Vonck J, Mills DJ, Meier T, Kühlbrandt W. 2018. Structure, mechanism, and regulation of the chloroplast ATP synthase. *Science* **360**(6389): eaat4318.

Hatakeyama Y, Ueno O. 2016. Intracellular position of mitochondria and chloroplasts in bundle sheath and mesophyll cells of C_3 grasses in relation to photorespiratory CO_2 loss. *Plant Production Science* **19**(4): 540-551.

Heckmann D, Schulze S, Denton A, Gowik U, Westhoff P, Weber Andreas PM, Lercher Martin J. 2013. Predicting C_4 Photosynthesis Evolution: Modular, Individually Adaptive Steps on a Mount Fuji Fitness Landscape. *Cell* **153**(7): 1579-1588.

Hermida-Carrera C, Kapralov MV, Galmés J. 2016. Rubisco catalytic properties and temperature response in crops. *Plant Physiology*: pp. 01846.02016.

Horton P, Murchie EH 2000. C4 photosynthesis in rice: some lessons from studies of C_3 photosynthesis in field-grown rice*. In: J.E. Sheehy PLM, Hardy B eds. *Studies in Plant Science*: Elsevier, 127-144.

Ishikawa N, Takabayashi A, Sato F, Endo T. 2016. Accumulation of the components of cyclic electron flow around photosystem I in C_4 plants, with respect to the requirements for ATP. *Photosynthesis Research*: 1-17.

Ivanov B, Asada K, Kramer DM, Edwards G. 2005. Characterization of photosynthetic electron transport in bundle sheath cells of maize. I. Ascorbate effectively stimulates cyclic electron flow around PSI. *Planta* **220**(4): 572-581.

Jurić I, González-Pérez V, Hibberd JM, Edwards G, Burroughs NJ. 2017. Size matters for single-cell C4 photosynthesis in Bienertia. *Journal of Experimental Botany* **68**(2): 255-267.

Kajala K, Covshoff S, Karki S, Woodfield H, Tolley BJ, Dionora MJA, Mogul RT, Mabilangan AE, Danila FR, Hibberd JM, et al. 2011. Strategies for engineering a two-celled C4 photosynthetic pathway into rice. *Journal of Experimental Botany* **62**(9): 3001-3010.

Kanai R, Edwards GE 1999. The biochemistry of C_4 photosynthesis. In: Sage RF, Monson RK eds. *C4 plant biology*. San Diego: Academic Press.

Keerberg O, Pärnik T, Ivanova H, Bassüner B, Bauwe H. 2014. C_2 photosynthesis generates about 3-fold elevated leaf CO_2 levels in the C_3–C_4 intermediate species Flaveria pubescens. *Journal of Experimental Botany* **65**(13): 3649-3656.

King JL, Edwards GE, Cousins AB. 2012. The efficiency of the CO2-concentrating mechanism during single-cell C_4 photosynthesis. *Plant, Cell & Environment* **35**(3): 513-523.

Kromdijk J, Ubierna N, Cousins AB, Griffiths H. 2014. Bundle-sheath leakiness in C_4 photosynthesis: a careful balancing act between CO2 concentration and assimilation. *Journal of Experimental Botany* **65**(13): 3443-3457.

Leakey ADB, Ainsworth EA, Bernacchi CJ, Zhu X, Long SP, Ort DR 2012. Photosynthesis in a CO_2-Rich Atmosphere. In: Eaton-Rye JJ, Tripathy BC, Sharkey TD eds. *Photosynthesis: Plastid Biology, Energy Conversion and Carbon Assimilation*. Dordrecht: Springer Netherlands, 733-768.

Leakey ADB, Bernacchi CJ, Dohleman FG, Ort DR, Long SP. 2004. Will photosynthesis of maize (Zea mays) in the US Corn Belt increase in future [CO2] rich atmospheres? An analysis of diurnal courses of CO_2 uptake under free-air concentration enrichment (FACE). *Global Change Biology* **10**(6): 951-962.

Leegood RC. 2013. Strategies for engineering C_4 photosynthesis. *Journal of Plant Physiology* **170**(4): 378-388.

Li T, Hasegawa T, Yin X, Zhu Y, Boote K, Adam M, Bregaglio S, Buis S, Confalonieri R, Fumoto T. 2015. Uncertainties in predicting rice yield by current crop models under a wide range of climatic conditions. *Global Change Biology* **21**(3): 1328-1341.

Long SP, Ainsworth EA, Leakey ADB, Nösberger J, Ort DR. 2006. Food for thought: Lower-than-expected crop yield stimulation with rising CO_2 concentrations. *Science* **312**(5782): 1918-1921.

Long Stephen P, Marshall-Colon A, Zhu X-G. 2015. Meeting the Global Food Demand of the Future by Engineering Crop Photosynthesis and Yield Potential. *Cell* **161**(1): 56-66.

Lundgren MR, Osborne CP, Christin P-A. 2014. Deconstructing Kranz anatomy to understand C_4 evolution. *Journal of Experimental Botany* **65**(13): 3357-3369.

Meyer M, Griffiths H. 2013. Origins and diversity of eukaryotic CO_2-concentrating mechanisms: lessons for the future. *Journal of Experimental Botany* **64**(3): 769-786.

Monson RK, Moore Bd. 1989. On the significance of C_3—C_4 intermediate photosynthesis to the evolution of C4 photosynthesis. *Plant, Cell & Environment* **12**(7): 689-699.

Monteith JL. 1978. Reassessment of Maximum Growth-Rates for C_3 and C_4 Crops. *Experimental Agriculture* **14**(1): 1-5.

Munekage YN, Eymery F, Rumeau D, Cuine S, Oguri M, Nakamura N, Yokota A, Genty B, Peltier G. 2010. Elevated Expression of PGR5 and NDH-H in Bundle Sheath Chloroplasts in C_4 Flaveria Species. *Plant and Cell Physiology* **51**(4): 664-668.

Osmond C, Smith F 1976. Symplastic transport of metabolites during C_4-photosynthesis. *Intercellular communication in plants: Studies on plasmodesmata*: Springer, 229-241.

Paleari L, Movedi E, Cappelli G, Wilson LT, Confalonieri R. 2017. Surfing parameter hyperspaces under climate change scenarios to design future rice ideotypes. *Global Change Biology*.

Pearcy RW, Ehleringer J. 1984. Comparative ecophysiology of C_3 and C_4 plants. *Plant, Cell & Environment* **7**(1): 1-13.

Pearcy RW, Gross LJ, He D. 1997. An improved dynamic model of photosynthesis for estimation of carbon gain in sunfleck light regimes. *Plant Cell and Environment* **20**(4): 411-424.

Pick TR, Brautigam A, Schluter U, Denton AK, Colmsee C, Scholz U, Fahnenstich H, Pieruschka R, Rascher U, Sonnewald U, et al. 2011. Systems Analysis of a Maize Leaf Developmental Gradient Redefines the Current C_4 Model and Provides Candidates for Regulation. *Plant Cell* **23**(12): 4208-4220.

Pignon CP, Jaiswal D, McGrath JM, Long SP. 2017. Loss of photosynthetic efficiency in the shade. An Achilles heel for the dense modern stands of our most productive C_4 crops? *Journal of Experimental Botany* **68**(2): 335-345.

Quirk J, Bellasio C, Johnson DA, Osborne CP, Beerling DJ. 2018. C_4 savanna grasses fail to maintain assimilation in drying soil under low CO_2 compared with C_3 trees despite lower leaf water demand. *Functional Ecology* **33**(3): 388-398.

Retta M, Ho QT, Yin X, Verboven P, Berghuijs HNC, Struik PC, Nicolaï BM. 2016. A two-dimensional microscale model of gas exchange during photosynthesis in maize (Zea mays L.) leaves. *Plant Science* **246**(Supplement C): 37-51.

Rogers A, Medlyn BE, Dukes JS, Bonan G, Caemmerer S, Dietze MC, Kattge J, Leakey ADB, Mercado LM, Niinemets Ü, et al. 2017. A roadmap for improving the representation of photosynthesis in Earth system models. *New Phytologist* **213**(1): 22-42.

Sage RF, Khoshravesh R. 2016. Passive CO_2 concentration in higher plants. *Current Opinion in Plant Biology* **31**: 58-65.

Sage TL, Sage RF. 2009. The Functional Anatomy of Rice Leaves: Implications for Refixation of Photorespiratory CO_2 and Efforts to Engineer C_4 Photosynthesis into Rice. *Plant and Cell Physiology* **50**(4): 756-772.

Sander R. 2015. Compilation of Henry's law constants (version 4.0) for water as solvent. *Atmospheric Chemistry & Physics* **15**(8).

Schlüter U, Bräutigam A, Droz J-M, Schwender J, Weber AP. The role of alanine and aspartate aminotransferases in C4 photosynthesis. *Plant Biology* **0**(ja).

Schlüter U, Denton AK, Bräutigam A. 2016. Understanding metabolite transport and metabolism in C_4 plants through RNA-seq. *Current Opinion in Plant Biology* **31**: 83-90.

Schmitt MR, Edwards GE. 1981. Photosynthetic Capacity and Nitrogen Use Efficiency of Maize, Wheat, and Rice: A Comparison Between C_3 and C_4 Photosynthesis. *Journal of Experimental Botany* **32**(3): 459-466.

Sheehy JE, ed. 2007. *Charting New Pathways to C_4 Rice*. Singapore: World Scientific Publishing.

Snaydon RW. 1991. The Productivity of C_3 and C_4 Plants - a Reassessment. *Functional Ecology* **5**(3): 321-330.

Song Q, Zhang G, Zhu X-G. 2013. Optimal crop canopy architecture to maximise canopy photosynthetic CO_2 uptake under elevated CO_2 – a theoretical study using a mechanistic model of canopy photosynthesis. *Functional Plant Biology* **40**(2): 108-124.

Sowiński P 2013. Characteristics of Symplasmic Transport. In: Sokołowska K, Sowiński P eds. *Symplasmic Transport in Vascular Plants*: Springer New York, 1-39.

Sowinski P, Szczepanik J, Minchin PEH. 2008. On the mechanism of C_4 photosynthesis intermediate exchange between Kranz mesophyll and bundle sheath cells in grasses. *Journal of Experimental Botany* **59**(6): 1137-1147.

Sun W, Ubierna N, Ma J-Y, Walker B, Kramer D, Cousins AB. 2014. The coordination of C_4 photosynthesis and the CO_2 concentrating mechanism in Zea mays and Miscanthus × giganteus in response to transient changes in light quality. *Plant Physiology* **164**(3): 1283-1292.

Takeuchi Y, Akagi H, Kamasawa N, Osumi M, Honda H. 2000. Aberrant chloroplasts in transgenic rice plants expressing a high level of maize NADP-dependent malic enzyme. *Planta* **211**(2): 265-274.

Taylaran RD, Ozawa S, Miyamoto N, Ookawa T, Motobayashi T, Hirasawa T. 2009. Performance of a High-Yielding Modern Rice Cultivar Takanari and Several Old and New Cultivars Grown with and without Chemical Fertilizer in a Submerged Paddy Field. *Plant Production Science* **12**(3): 365-380.

Taylor SH, Hulme SP, Rees M, Ripley BS, Ian Woodward F, Osborne CP. 2010. Ecophysiological traits in C_3 and C_4 grasses: a phylogenetically controlled screening experiment. *New Phytologist* **185**(3): 780-791.

Tazoe Y, Hanba YT, Furumoto T, Noguchi K, Terashima I. 2008. Relationships between quantum yield for CO_2 assimilation, activity of key enzymes and CO_2 leakiness in Amaranthus cruentus, a C_4 dicot, grown in high or low light. *Plant and Cell Physiology* **49**(1): 19-29.

Ubierna N, Sun W, Cousins AB. 2011. The efficiency of C_4 photosynthesis under low light conditions: assumptions and calculations with CO_2 isotope discrimination. *Journal of Experimental Botany* **62**(9): 3119-3134.

Ubierna N, Sun W, Kramer DM, Cousins AB. 2013. The Efficiency Of C_4 Photosynthesis Under Low Light Conditions In Zea mays, Miscanthus X giganteus And Flaveria bidentis. *Plant, Cell & Environment* **36**: 365-381.

Vialet-Chabrand S, Matthews JSA, Brendel O, Blatt MR, Wang Y, Hills A, Griffiths H, Rogers S, Lawson T. 2016. Modelling water use efficiency in a dynamic environment: An example using Arabidopsis thaliana. *Plant Science* **251**: 65-74.

Vollmar M, Schlieper D, Winn M, Büchner C, Groth G. 2009. Structure of the c14 Rotor Ring of the Proton Translocating Chloroplast ATP Synthase. *Journal of Biological Chemistry* **284**(27): 18228-18235.

von Caemmerer S. 1989. A model of photosynthetic CO_2 assimilation and carbon-isotope discrimination in leaves of certain C_3–C_4 intermediates. *Planta* **178**(4): 463-474.

von Caemmerer S. 2000. *Biochemical models of leaf Photosynthesis*. Collingwood: CSIRO Publishing.

von Caemmerer S, Furbank RT. 2003. The C_4 pathway: an efficient CO_2 pump. *Photosynthesis Research* **77**(2-3): 191-207.

Wang P, Kelly S, Fouracre JP, Langdale JA. 2013. Genome-wide transcript analysis of early maize leaf development reveals gene cohorts associated with the differentiation of C_4 Kranz anatomy. *The Plant Journal* **75**(4): 656-670.

Wang S, Tholen D, Zhu X-G. 2017. C_4 photosynthesis in C_3 rice: a theoretical analysis of biochemical and anatomical factors. *Plant, Cell & Environment* **40**(1): 80-94.

Wang Y, Bräutigam A, Weber APM, Zhu X-G. 2014. Three distinct biochemical subtypes of C_4 photosynthesis? A modelling analysis. *Journal of Experimental Botany*.

Warneck P, Williams J 2012. Rate Coefficients for Gas-Phase Reactions. *The Atmospheric Chemist's Companion*: Springer, 227-269.

Way DA, Oren R, Kim HS, Katul GG. 2011. How well do stomatal conductance models perform on closing plant carbon budgets? A test using seedlings grown under current and elevated air temperatures. *Journal of Geophysical Research: Biogeosciences (2005–2012)* **116**(G4).

Weber APM, von Caemmerer S. 2010. Plastid transport and metabolism of C_3 and C_4 plants — comparative analysis and possible biotechnological exploitation. *Current Opinion in Plant Biology* **13**(3): 256-264.

Wei J-C, Wang R-L, Cheng G-Y. 1994. Studies on the kinetic properties of ribulose-1, 5-bisphosphate carboxylase from of F1 hybrid rice. *Acta Phytophisiologica Sinica* **20**: 55-60.

Wu A, Doherty A, Farquhar GD, Hammer GL. 2017. Simulating daily field crop canopy photosynthesis: an integrated software package. *Functional Plant Biology* **45**(3): 362-377.

Yamori W, Shikanai T. 2016. Physiological Functions of Cyclic Electron Transport Around Photosystem I in Sustaining Photosynthesis and Plant Growth. *Annual review of plant biology* **67**(1): 81-106.

Yin X, Struik PC. 2015. Constraints to the potential efficiency of converting solar radiation into phytoenergy in annual crops: from leaf biochemistry to canopy physiology and crop ecology. *Journal of Experimental Botany* **66**(21): 6535-6549.

Yin X, Struik PC. 2017. Can increased leaf photosynthesis be converted into higher crop mass production? A simulation study for rice using the crop model GECROS. *Journal of Experimental Botany* **68**(9): 2345-2360.

Yin X, Struik PC, Romero P, Harbinson J, Evers JB, Van Der Putten PEL, Vos JAN. 2009. Using combined measurements of gas exchange and chlorophyll fluorescence to estimate parameters of a biochemical C_3 photosynthesis model: a critical appraisal and a new integrated approach applied to leaves in a wheat (Triticum aestivum) canopy. *Plant, Cell & Environment* **32**(5): 448-464.

Yin X, van der Putten PEL, Driever SM, Struik PC. 2016. Temperature response of bundle-sheath conductance in maize leaves. *Journal of Experimental Botany* **67**(9): 2699-2714.

Yin XY, Struik PC. 2012. Mathematical review of the energy transduction stoichiometries of C_4 leaf photosynthesis under limiting light. *Plant Cell and Environment* **35**(7): 1299-1312.

Tables.

Table 1. Acronyms, definitions, values, and units used.

Symbol / Acronym	Definition	Values / Units	Source
A	Net assimilation	μmol m^{-2} s^{-1}	output
a_t	Total concentration of adenylates in chloroplast	12.7 mmol m^{-2}	Farquhar and Wong (1984)
BS	Bundle sheath		
C_{BS}	CO_2 concentration in the BS	μmol mol^{-1}	output
CCM	Carbon concentrating mechanism		
CEF	Cyclic electron flow		
C_M	CO_2 concentration in the M	μmol mol^{-1}	variable, iteratively found
D_S	Leaf to boundary layer water mole fraction gradient in the light (10 × VPD in kPa)	10 mmol H_2O mol air $^{-1}$	gas exchange
D_{S0}	Leaf to boundary layer water mole fraction gradient in the dark (10 × VPD in kPa)	8.6 mmol H_2O mol air $^{-1}$	gas exchange
E_t	Total concentration of Rubisco sites	6.7 mmol m^{-2}	adjusted from Farquhar and Wong (1984) by fitting gas exchange data
$f_{C\ Rubisco}$	Parameter defining the fraction of actual Rubisco carboxylation in BS relative to leaf–level	dimensionless	set to equal V_{CBS}/V_C output of the enzyme–limited model
f_{Cyc}	Fraction of J_1 following CEF	dimensionless	fitted to max A
f_{NDH}	Fraction of CEF through the NDH complex	0 (C_3 and C_2); 0.2 and 0‡ (C_2+C_4); 0.4 and 0‡ (C_4)	assigned
f_{PPDK}	Parameter defining the fraction of PPDK activity in the BS relative to leaf–level	0	assigned
f_{PR}, f_{CS},	Parameter defining the fraction of activity in BS relative to leaf–level, of phosphoglycerate reduction rate, and carbohydrate synthesis	0 (variable for the simulations of Figure 6B and 6D)	assigned
$f_{Pseudocyc}$	Fraction of J_1 following used by alternative sinks of electrons like nitrate reduction and the water–water cycle	0.1	assigned (Yin & Struik, 2012)
f_Q	Fraction of J_1 going through the Q–Cycle	1	Yin and Struik (2012)
f_{RLIGHT},	parameter defining the fraction of respiration in the light in BS relative to leaf–level	0 (C_3); 0.2 (C_2); 0.5 (C_2+C_4, and C_4)	(von Caemmerer, 1989; von Caemmerer, 2000)
g_{BS}	Bundle sheath conductance to CO_2 diffusion	0.00287† mol m^{-2} s^{-1}	Yin *et al.* (2016)
GDC	Glycine decarboxylase		
g_M	Mesophyll conductance to CO_2 diffusion	0.26† mol m^{-2} s^{-1}	gas exchange
g_{S0}	Stomatal conductance in the dark	0.047 mol CO_2 m^{-2} s^{-1}	gas exchange
h	Stoichiometry of ATP synthase: protons required to synthesize ATP	4.67 protons / ATP	Vollmar *et al.* (2009); Hahn *et al.* (2018)
I, I_1, I_2, $I_{1\,0}$, $I_{2\,0}$	Light absorbed by PSI and PSII, by PSI, by PSII, by PSI when f_{Cyc}=0, by PSII when f_{Cyc}=0, respectively	μmol m^{-2} s^{-1}	output
J_1, J_2	Electron flow through PSI, and PSII, respectively	μmol m^{-2} s^{-1}	output
J_{ATP}	Total leaf–level ATP production rate	μmol m^{-2} s^{-1}	output
J_{NADPH}	Total leaf–level NADPH production rate	μmol m^{-2} s^{-1}	output
J_{SAT}	*PPFD* saturated electron transport rate	310† μmol m^{-2} s^{-1}	chlorophyll fluorescence
K_C	Rubisco Michaelis–Menten constant for CO_2 in the liquid phase	8† μM	(Wei *et al.*, 1994; von Caemmerer, 2000; Galmés *et al.*, 2016; Hermida-Carrera *et al.*, 2016)
K_h	Effective hydraulic conductance from the soil to the epidermis	12 mmol H2O m^{-2} s^{-1} MPa^{-1}	Bellasio *et al.* (2017)
$KhCO_2$	volatility of CO_2	30.3† μbar μM^{-1}	Sander (2015)
KhO_2	volatility of O_2	833.3† μbar μM^{-1}	Warneck and Williams (2012)
K_O	Rubisco Michaelis–Menten constant for O_2 in the liquid phase	335† μM	von Caemmerer (2000)
M	Mesophyll		
NDH	NAD(P)H Dehydrogenase–like (complex)		
O_M, O_{BS}	O_2 concentration in M cells or BS cells	O_M is 210000 or 21000 μmol mol^{-1} O_{BS} is calculated	O_M is assigned O_{BS} is output
p	Concentration of photophosphorylation sites	7.5 mmol m^{-2}	adjusted from Farquhar and Wong (1984) by fitting gas exchange data
PEPC	Phospho*enol*pyruvate carboxylase		
PEPCK	Phospho*enol*pyruvate carboxykinase		
PPDK	Pyruvate phosphate dikinase		

PPFD	Photosynthetic photon flux density	μmol m^{-2} s^{-1}	assigned
R_{LIGHT} $R_{LIGHT\ BS}$, $R_{LIGHT\ M}$	Respiration in the light, leaf–level, in the BS or in the M, respectively	R_{LIGHT} is 0.8† μmol m^{-2} s^{-1}	gas exchange, 0.5 is the assumed fraction of BS respiration relative to total
r_{PEPCK}	input parameter defining the activity of PEPCK relative to V_P	0	assigned
Rubisco	Ribulose bisphosphate carboxylase oxygenase		
RuBP	Ribulose–1,5–bisphosphate		
s	lumped energy conversion coefficient (Yin *et al.*, 2009)	0.38 e^-/quanta	gas exchange
$S_{C/O}$	Rubisco specificity	2800† μbar/μbar (gas) or 102† mol mol^{-1} (liq)	gas exchange
$V_{C\ MAX}$, V_C, $V_{C\ BS}$, $V_{C\ M}$	Rubisco carboxylation rate, CO_2 saturated, leaf–level, in the BS, in the M, respectively	V_{CMAX} is 93† μmol m^{-2} s^{-1}	V_{CMAX} by gas exchange, or output
V_O, $V_{O\ BS}$, $V_{O\ M}$	Rubisco oxygenation rate, total, in the BS or in the M, respectively	μmol m^{-2} s^{-1}	output
$V_{P(J)}$	Leaf–level actual phospho*enol*pyruvate carboxylation rate, inputs to the light–limited model	0 (C_3 and C_2); 0.075J_{ATP} (C_2+C_4); 0.2J_{ATP} (C_4) μmol m^{-2} s^{-1} (variable for the simulations in Figure 6)	assigned (von Caemmerer, 2000)
$V_{P\ MAX}$	CO_2 saturated phospho*enol*pyruvate carboxylation rate	0 (C_3 and C_2); 0.1J_{SAT} (C_2+C_4); 0.3J_{SAT} (C_4) μmol m^{-2} s^{-1}	assigned
V_r	Potential pool size of RuBP	150 mmol m^{-2}	Farquhar and Wong (1984)
$Y(I)_{LL}$,	Yield of PSI extrapolated under zero *PPFD*	1	Yin and Struik (2012)
$Y(II)_{LL}$	Yield of PSII extrapolated under zero *PPFD*	0.75	chlorophyll fluorescence
$Y(II)_{MOD}$	Yield of PSII modelled empirically by a non–rectangular hyperbola	dimensionless	output
α	parameter scaling BS O_2 evolution to net assimilation attributed to BS activity	1	von Caemmerer (1989)
Γ^*	Half the reciprocal Rubisco specificity $\gamma* = \frac{1}{2S_{C/O}}$	dimensionless	output
θ	Curvature of the non–rectangular hyperbola used to model the light–dependence of *Y(II)*	0.5	gas exchange
θ_A	Curvature of the non–rectangular hyperbola used to smooth the combination of light–limited and enzyme–limited models	0.95	Buckley *et al.* (2016)
ξ_{GDC}	Specifies the fraction of V_{OM} which is decarboxylated in the BS.	0 (C_3) and 1 (C_2, C_2+C_4, and C_4)	Sage and Khoshravesh (2016)
χ_I	Fraction of *I* shifting from PSII to PSI upon engagement of CEF	dimensionless	output
$\chi_{Rubisco}$	parameter defining the fraction of V_{CMAX} in BS relative to leaf–level	dimensionless	fitted to maximise *A*
$\chi_S\beta$	Parameter lumping turgor to conductance scaling factor and the hydromechanical / biochemical response parameter	0.055 mol air $mmol^{-1}$ ATP s^{-1} MPa^{-1}	fitted to gas exchange data
ψ_{Soil}, ψ_{Soil0}	Soil water potential in the light or in the dark respectively	0 MPa	assigned
π_e	Epidermal osmotic pressure	1.2 MPa	Bellasio *et al.* (2017)

† The value shown is at 25 °C but the quantity was made temperature–dependent; ‡ Alternative scenarios in Figure 4

Figures.

Figure 1. Modelling framework. Blue boxes show inputs while orange boxes show outputs; grey boxes represent submodels. Inputs with a thick blue outline are made temperature–dependent. Submodels contoured in red are originally developed for this work. Photosynthetic photon flux density (*PPFD*) is an input to the electron transport submodel to calculate the total ATP production rate (J_{ATP}) and the total NADPH production rate (J_{NADPH}). These and dummy values for CO_2 concentration at the M carboxylating sites (C_M) are fed into the light– and enzyme–limited submodels (Dashed boxes). The outputs from the photosynthesis submodels are used to calculate chloroplastic ATP concentration (τ) and a smoothed combination of the submodels is fed into a stoichiometric submodel to calculate fluxes and reaction rates. τ is used in the stomatal submodel along with inputs for soil water potential (Ψ_{Soil}) and evaporative demand (D_S). The output stomatal conductance (g_S) is used to calculate CO_2 concentration in the sub–stomatal cavity (C_i) from external CO_2 concentration (C_a) and in turn used to calculate C_M, which is iterated. See Table 1 for more abbreviations.

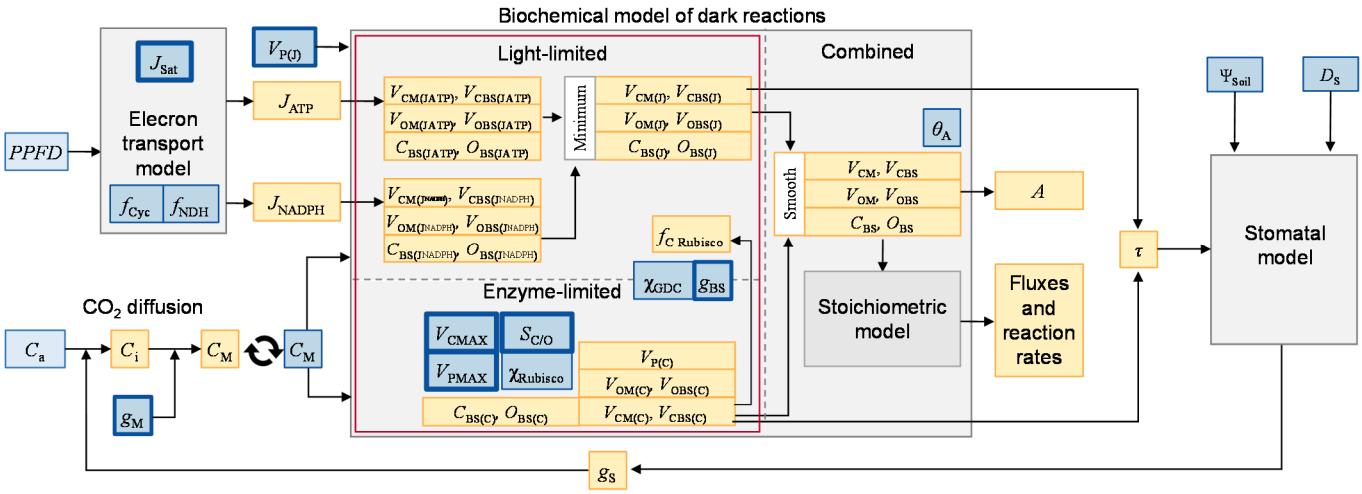

Figure 2. Assimilation and stomatal conductance measured on rice and corresponding simulations for a C_3 photosynthetic type. Panel **A**: light–response curves. Symbols show the response of assimilation (*A*) to decreasing light intensity (*PPFD*) measured under ambient O_2 (closed circles) or 2% O_2 (open circles). Lines show modelled assimilation under ambient O_2 (solid line) or 2% O_2 (dashed line). Panel **B**: A/C_i curves. Symbols show the measured *A* at varying levels of CO_2 concentration in the substomatal cavity, C_i, under ambient and low O_2. Lines show the corresponding simulations. Panel **C**: measured and simulated response of stomatal conductance (g_S) to *PPFD* under ambient and low O_2. Panel **D**: measured and simulated response of stomatal conductance (g_S) to external CO_2 concentration, *C*a, under ambient and low O_2. Symbols show mean ± SE, n=4. For simulated A/C_i curves, C_a was set at 16 levels [between 20 and 1000 µmol mol^{-1}] while *PPFD* was set at 1200 µmol m^{-2} s^{-1}, the same used for gas exchange measurements. For simulated *A/PPFD* curves, *PPFD* was set at 18 levels [between 1 and 1500 µmol m^{-2} s^{-1}] and C_a was set at 400 µmol mol^{-1}. Temperature was 25° C while $\chi_{Rubisco}$ and f_{Cyc} were fitted for each combination of inputs.

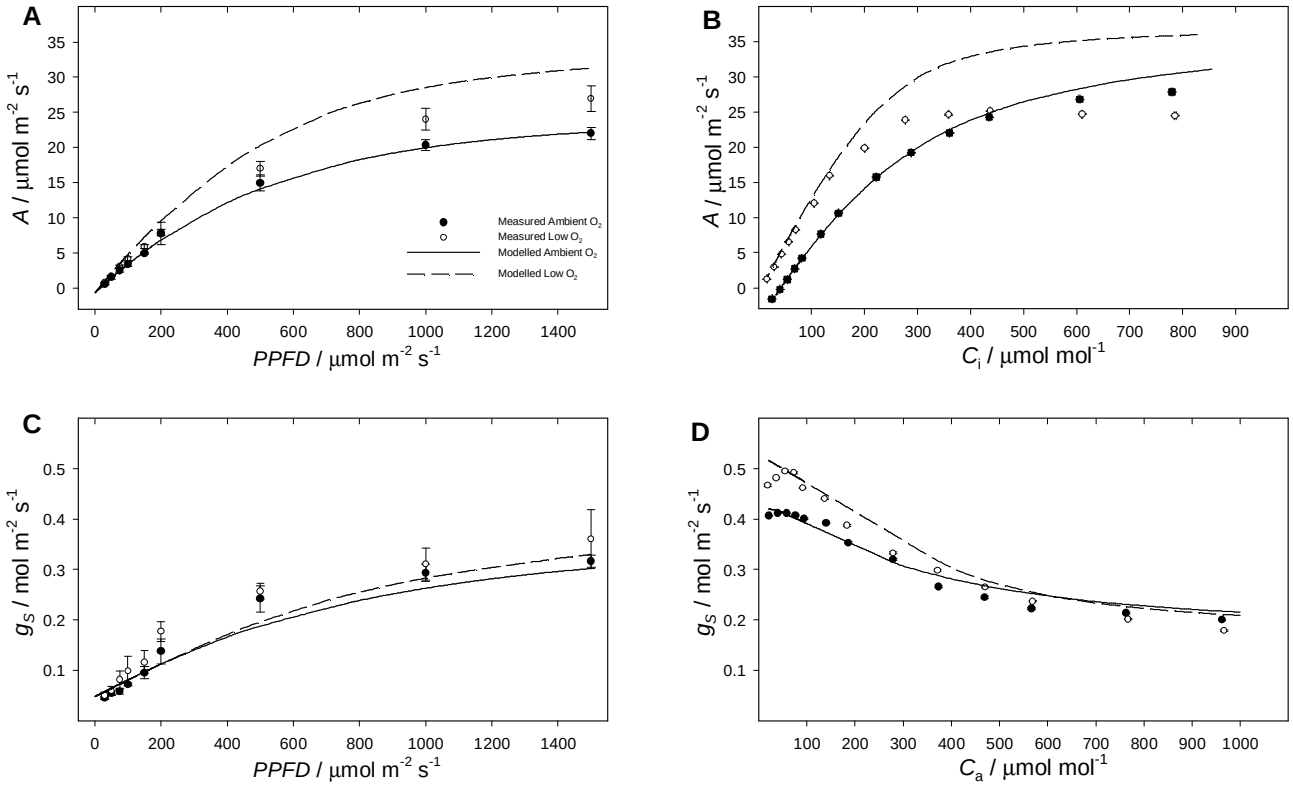

Figure 3. Simulated *A*–response curves. Compared model output for the four photosynthetic types in response to changes in *PPFD* (Left) or C_a (Right) varied in the same steps of curves above. Four different photosynthetic types were simulated in a best case scenario for bioengineering whereby the NDH complex is expressed (f_{NDH}>0), f_{Cyc} and $\chi_{Rubisco}$ are optimal (fitted to max *A*): C_3 (black solid line), representing the measured plants; C_2 (orange dashed line); C_2+C_4 (red solid line); and C_4 (blue dash–dot line). Panels **A** and **B**: net assimilation. Panels **C** and **D**: stomatal conductance. Panels **E** and **F**: CO_2 concentration in the BS. Panels **G** and **H**: Rubisco rate of oxygenation to carboxylation V_O/V_C. Panels **I** and **J**: fraction of Rubisco carboxylating activity in the BS, relative to total.

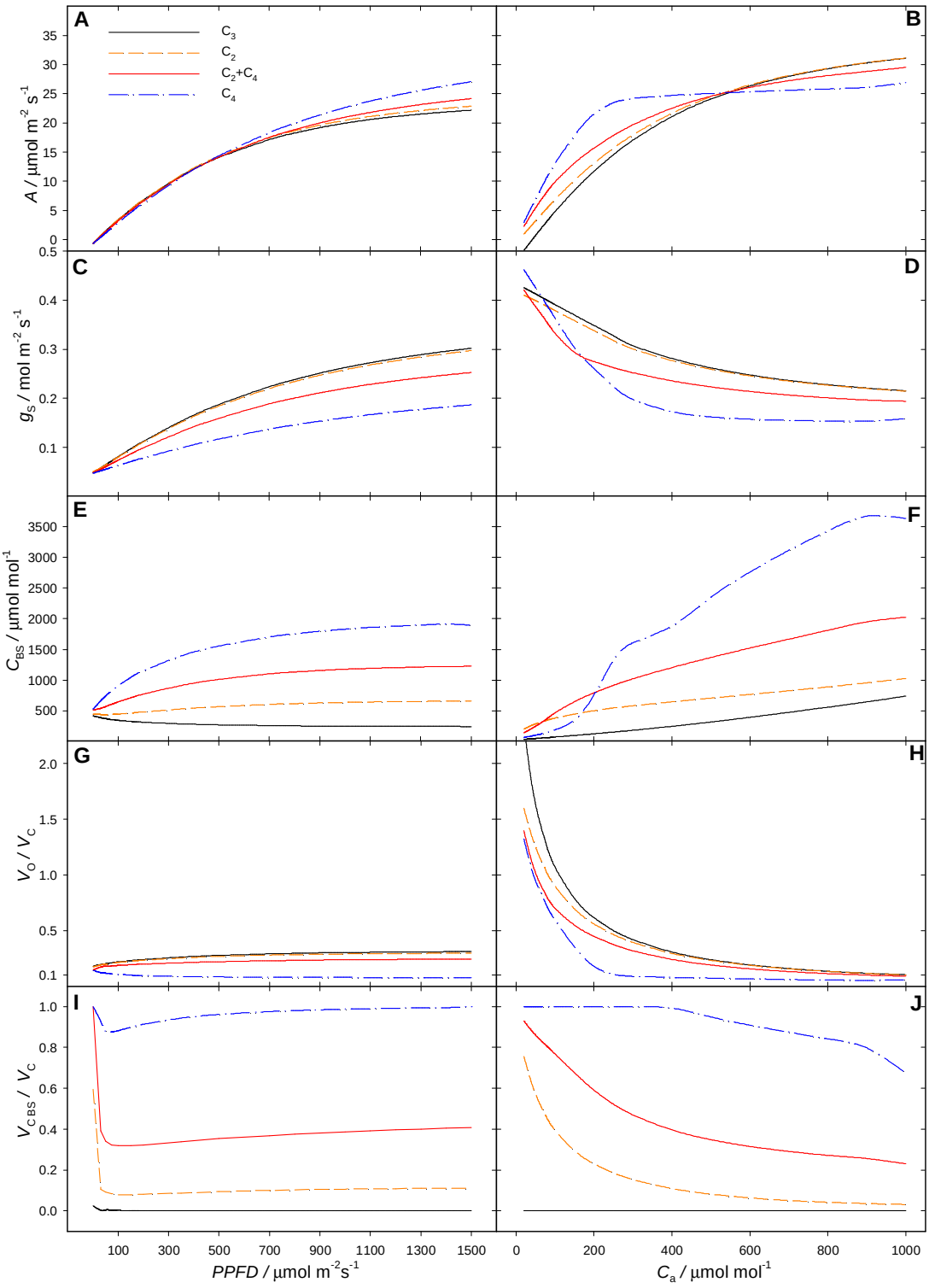

Figure 4. Assimilation in the best case scenario. Gains were calculated for 100 combinations of temperature (varied in 10 steps from 16 °C to 43 °C) and *PPFD* (varied in 10 steps from 1 to 1500 µmol m^{-2} s^{-1}), under a C_a of 400 µmol mol^{-1} (top row), or in 100 combinations of *C*a (varied in 10 steps from 150 to 690 µmol mol^{-1}) and temperature (as above), under a *PPFD* of 700 µmol m^{-2} s^{-1} (bottom row) in a best case scenario whereby electron transport processes fully accommodate for the presence of different types of CCM (f_{NDH}>0, f_{Cyc} is fitted) and Rubisco is optimally allocated ($\chi_{Rubisco}$ is fitted). The gain was expressed as relative to C_3 assimilation (Panels **A** and **E**), for C_2 (Panel **B** and **F**) C_2+C_4 (panel **C** and **G**) and C_4 (panel **D** and **H**).

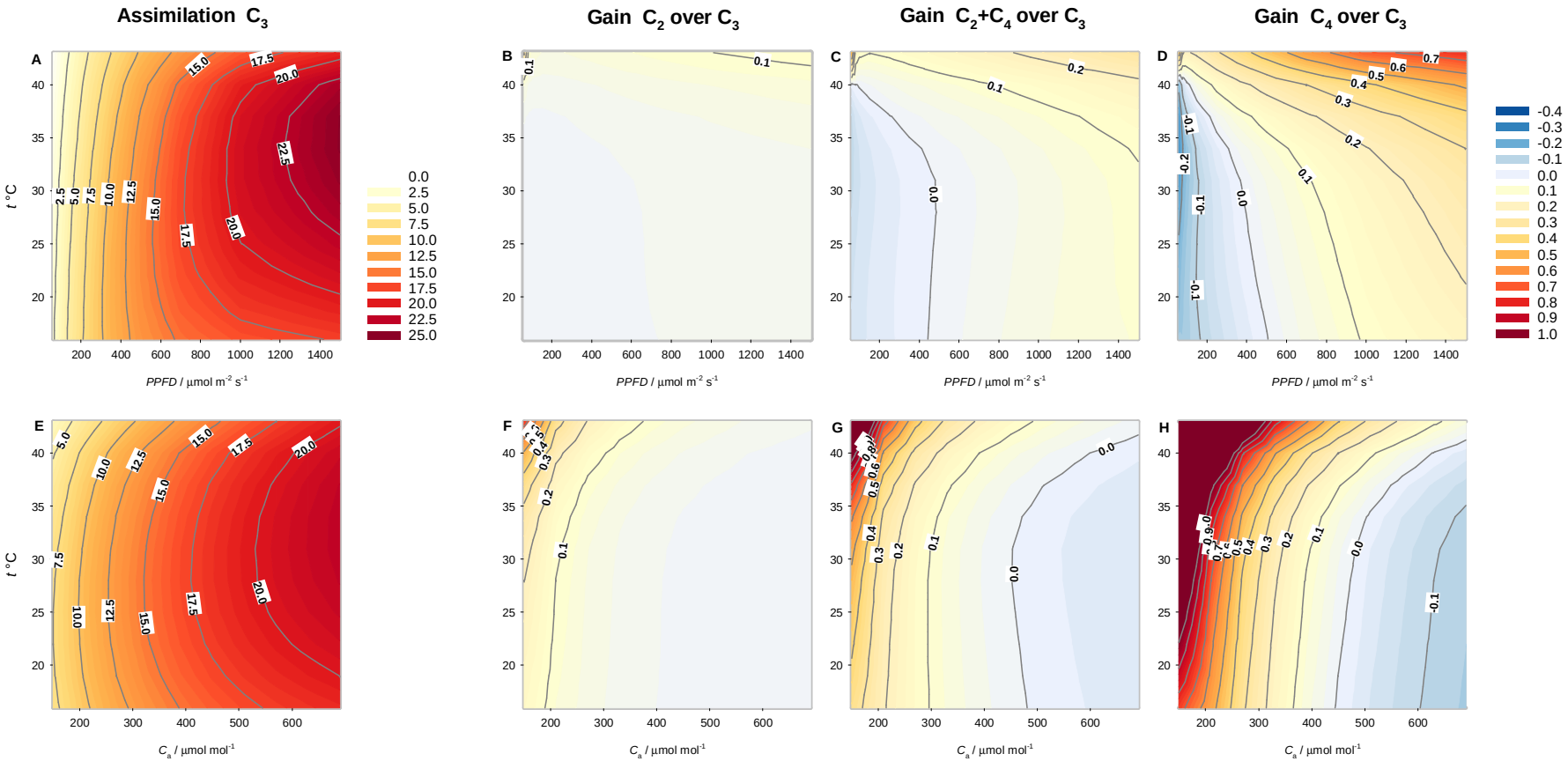

Figure 5. Assimilation in alternative scenarios. Gains were calculated in the temperature × *PPFD* space, under a C_a of 400 µmol mol^{-1}, expressed as relative to C_3 assimilation (Figure 4). Panels **A**, **B**, and **C** show a less optimistic scenario whereby the activity of the NDH complex remain at C_3 levels, modelled by setting f_{NDH} at zero for all photosynthetic types. Panels **D**, **E** and **F** show a pessimistic scenario whereby in addition to f_{NDH}=0, the fraction of cyclic electron flow (f_{Cyc}) was set at C_3 levels for all photosynthetic types.

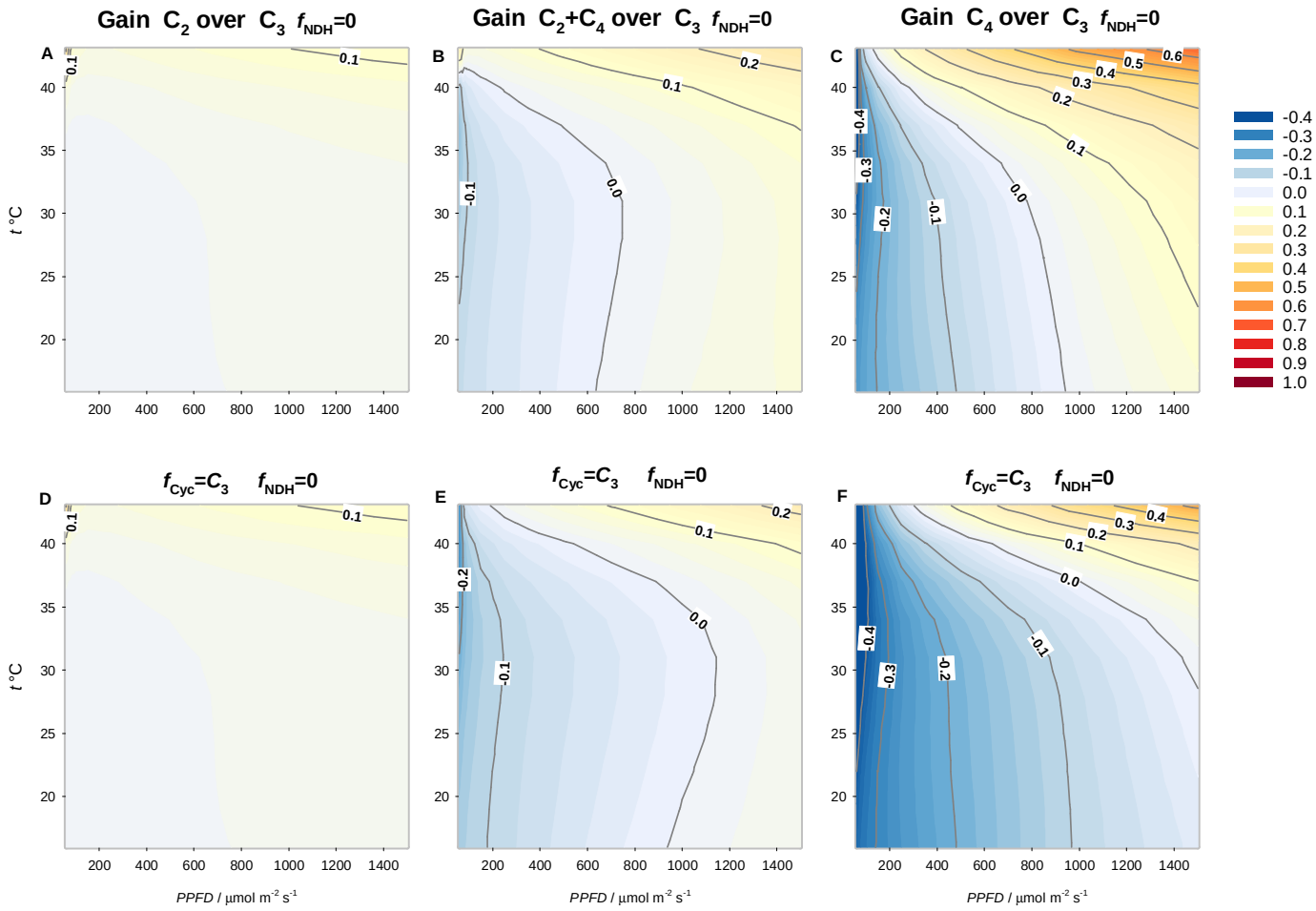

Figure 6. Modelled fluxes between the M and the BS at increasing levels of C_4 engagement. In this simulation the C_4 CCM was increasingly upregulated by manipulating PEPC activity ($V_{P\,(J)}$, µmol m^{-2} s^{-1}) to increase from 0 to 0.2 J_{ATP} to represent the C_2 to C_4 continuum (from left to right of each panel). Panel **A** simulates a scenario of minimum ATP demand in BS obtained by setting r_{PEPCK}, f_{PR}, f_{CS} and f_{PPDK} at zero; other inputs represented the operational conditions of *PPFD* 700 µmol m^{-2} s^{-1}, 25 °C, and C_a=350 µmol mol^{-1}. Panel **B** simulates a scenario of minimum sum of squared flow rates between BS and M obtained by fitting f_{PR}, and f_{CS}. In these conditions the ATP demand in BS increased substantially, and is shown as relative to the ATP demand in the M in panels **C** and **D**. The flux is considered positive when in the M to BS direction for MAL, ASP, DHAP, and GLY, and in the opposite direction for the other metabolites (Figure S1). Note the different scaling of *y*–axes.